Electric Power Systems Research 163 (2018) 133–139

Contents lists available at ScienceDirect

Electric Power Systems Research

journal homepage: www.elsevier.com/locate/epsr

A dynamic corona model for EMTP computation of multiple and non-standard impulses on transmission lines using a type-94 circuit component

Zahira Anane[a], Abdelhafid Bayadi[a,*], Noureddine Harid[b]

[a] Electrical Engineering Department, Faculty of Technology, Ferhat ABBAS University of Setif 1, Setif, Algeria
[b] Electrical and Computer Engineering Department, Khalifa University of Science and Technology, P.O. Box 2533, Abu Dhabi, United Arab Emirates

ARTICLE INFO

Keywords:
Corona model
Q–V characteristics
Overvoltages
Insulation coordination
ATP/EMTP

ABSTRACT

In this paper, a new non-linear corona model for computation of overvoltages of standard and non-standard oscillatory shape is proposed and implemented in a new model in ATP-EMTP using MODELS simulation language. The corona model is solved simultaneously with the rest of simulated system interacting with it as a circuit element; this is accomplished by using the model with a type-94 circuit component. The model can be used to compute the lightning overvoltage that propagates on overhead transmission lines.

The model computes the position of the corona space charge generated around the conductor to its diffusion at the conductor surface. An analysis for the computed results is made with an emphasis on the differences between the Q–V curves under impulse overvoltages of lightning, switching, oscillatory, and multiple-impulse type. Charge, electric field and voltage are related macroscopically in the model. The proposed model is verified by a comparison of the simulation results with measurements results available in the literature.

1. Introduction

In high voltage transmission lines, the corona phenomenon generates light, audible noise, radio noise, conductor vibration, ozone, and causes a loss of energy [1–5]. When an overvoltage transient occurs on a line due to a lightning strike or switching operation, it propagates in both directions and can become harmful to line and station equipment. Proper insulation coordination studies must therefore be made to ensure that such overvoltages are effectively attenuated before they hit equipment terminals. In this respect, corona is known to have a beneficial effect since it helps in attenuating the energy contained in the travelling overvoltage. For transient analysis, corona has been interpreted as an increase in the line capacitance which can be considered as a non-linear function of the instantaneous voltage appearing on the overhead line and its rate of change [2]. For optimum design of equipment insulation, and to achieve effective insulation coordination, corona effects must therefore be accurately quantified.

Several decades work on this subject has been directed both towards experimental testing and theoretical modelling. Experimental investigations on attenuation and distortion of lightning surges, corona losses and the associated increase of overhead transmission lines capacitance have been extensively studied both on real lines of several kilometers [3–9], and in laboratories on conductor samples of a few tens of meters [10–15]. The increase in line capacitance was designated by some researchers as a dynamic capacitance, which can be determined from the charge–voltage characteristics as the rate of change of charge with voltage [4–6].

The theoretical efforts to approach this problem contain line circuit models and quite complex physical corona models based on the theory of the development of the corona mechanism [8,16–20]. These approaches may generally be limited as the selection of their parameters is based on tests under a specific overvoltage waveform. A number of corona models have been developed for simulating lightning transients on transmission lines [4–6], and very few of them are available to predict the charge–voltage Q–V curves under nonstandard lightning impulses [4]. With the increasing implementation of grid-connected renewable energy systems, and the introduction of HVDC links, additional challenges are brought with regards to overvoltage protection and insulation coordination. Future network configuration means that an overvoltage occurring on one system creates overvoltages of different shapes due to multiple reflections within the said system on one hand, and at the interfaces between adjacent networks on the other. Multiple lightning strikes are also likely to occur in the same location, and their impact on transmission lines is not well understood. Consideration of such non-standard overvoltage shapes and the associated corona dynamics have to be considered in studying the attenuation and distortion of the resulting waves propagating in these networks.

This paper describes a model to compute the corona charge

* Corresponding author at: Département d'Electrotechnique, Faculté de Technologie, Université Sétif 1, Algerie.
E-mail addresses: zahiraelect@yahoo.fr (Z. Anane), a_bayadi@yahoo.fr, a_bayadi@univ-setif.dz (A. Bayadi), nharid@pi.ac.ae (N. Harid).

https://doi.org/10.1016/j.epsr.2018.06.006
Received 8 March 2018; Received in revised form 25 May 2018; Accepted 7 June 2018

generated by overvoltage transients on transmission line conductors, considering the non-linear corona dynamic properties, the non-standard waveshapes and the case of multiple overvoltage surges. The new model computes the corona capacitance from the line geometry and corona characteristics, thus avoiding the need to carry out full-scale impulse tests. The model is applicable to practical configurations for which the electric field distribution, which governs the initiation of corona, can be found by standard numerical methods. The corona model, with the aid of a type-94 component and MODELS feature of the ATP-EMTP package, is solved simultaneously with the rest of power system interacting with it as a circuit element. This is done because complex networks and control systems of arbitrary structure can be simulated in EMTP, which is a suitable tool for lightning overvoltage analysis. Application of the proposed model to a coaxial-conductor configuration and a conductor above ground configuration is presented and analysed. The model is validated by comparing the computed results with the experimental results available in the literature.

2. Description of the corona model

The known physical properties of corona development in air are used for the present physical model for corona effect. The main assumptions of the model are as detailed in Ref. [6], and are summarized below:

- The field at the high-voltage conductor is limited to the corona inception field E_0 during corona discharge.
- The criterion for streamer propagation is $E > E_c$, where E is the field at the tip of the streamer, and E_c is the streamer propagation field which is dependent on the polarity of the voltage [19]. It takes the value of 5 kV/cm in positive polarity and 18 kV/cm in negative polarity.

2.1. Corona inception voltage

Impulse overvoltages occurring on transmission lines are likely to cause corona in most cases because the corona inception voltage is almost always exceeded. This voltage is an important parameter that design engineers normally consider for optimizing conductor dimensions and configurations of bundle conductors, and is equally important for overvoltage attenuation studies. Various empirical formulas have been proposed in the literature to calculate the inception voltage of cylindrical conductors [21–24]. The effect of conductor temperature on the corona inception voltage, although not considered in this study, is important and a study highlighting this effect has been reported in Ref. [25]. For example, the modified Peek formula is used for a coaxial-electrode configuration and is given by:

$$V_0 = 31\left(1 + \frac{0.308}{\sqrt{r_0}}\right) r_0 \ln\frac{r_b}{r_0}[\text{kV}] \tag{1}$$

where r_0 and r_b are inner and outer radius of the coaxial cylindrical conductors (in cm) respectively [15].

For a conductor-above-ground configuration, the following formula is used [19]:

$$V_0 = E_0 r_0\left(\frac{2h - r_0}{2h}\right)\ln\left(\frac{2h - r_0}{2h}\right)[\text{kV}] \tag{2}$$

where r_0 is the conductor radius (in cm) and h is the conductor height in m.

E_0 is the critical electric field for corona inception on the conductor surface in kV/cm, which is calculated by the following empirical expression [14,19,26]:

$$E_0 = 23.8m\left[1 + \frac{0.67}{r_0^{0.4}}\right]\left[kV/m\right] \tag{3}$$

m is the roughness factor of the conductor surface.

For the case of bundle conductors, the inception voltage may be approximately computed using (3) and a computation of the maximum pre-inception field at the conductor surface. Alternatively, an equivalent conductor may be considered, whose radius is given by Ref. [27].

$$r_{eq} = \sqrt[n]{n r_0 r_f^{n-1}} \tag{4}$$

n: number of elementary conductors
r_{eq} equivalent radius of bundle in [cm]
r_0 is the radius of elementary conductor; in [cm]
r_f is the geometric mean radius (GMR) of the bundle in [cm]

2.2. Corona space charge

It is supposed that the space charge is emitted in the form of infinitesimal circular shells expanding radially away from the conductor as soon as the electric field at the conductor surface exceeds the critical value. When the voltage reaches the inception value, the total charge at the conductor is equal to the critical value $Q_0(t)$

$$Q_0 = C_0 V_0[\text{C/m}] \tag{5}$$

where C_0 is the geometrical capacitance to ground of the conductor, given by (6) for the coaxial configuration and by (7) for the conductor above-ground configurations respectively:

$$C_0 = \frac{2\pi\varepsilon_0}{\ln\left[\frac{r_b}{r_0}\right]}[F/m] \tag{6}$$

$$C_0 = \frac{2\pi\varepsilon_0}{\ln\left[\frac{2h - r_0}{r_0}\right]}[F/m] \tag{7}$$

ε_0 is the air permittivity.

During the corona discharge, the total charge at each instant is computed as follows:

$$Q(t) = Q_c(t) + Q_0(t)[C/m] \tag{8}$$

where: $Q_c(t)$ is the additional space charge generated by the corona discharge around the conductor. For the two configurations adopted in this paper, this charge is given by:

- For the coaxial configuration:

$$Q_c(t) = 2\pi\varepsilon_0(\mathrm{r_c(t)E_c} - \mathrm{r_0E_0})[C/m] \tag{9}$$

- For the conductor above-ground configuration:

$$Q_c(t) = \pi\varepsilon_0 \mathrm{E_0} r_c(t)\frac{(2h - r_c(t))}{h}[C/m] \tag{10}$$

where
$\mathrm{E_c}$: is the streamer propagation field
$r_c(t)$: is the position (radius) of the corona shells

At each time step Δt, if the computed charge exceeds the critical value, a new charge shell is generated around the conductor and is displaced by the incremental movement of this new shell Δr(t) given by the boundary conditions of electric field and the applied voltage, as shown in Fig. 1. This displacement is computed using an iterative algorithm as

$$r(t + \Delta t) = r(t) + \Delta r \tag{11}$$

$$\text{And } \Delta r = \mu E(t)\Delta t \tag{12}$$

The total charge computed using (8) can be thought of charging two parallel capacitances: the geometrical capacitance to ground of the conductor, and an additional corona capacitance C_{cor}. The latter is referred to as the dynamic capacitance and is defined as the ratio between the space charge increment during time interval Δt and the applied voltage change during that time:

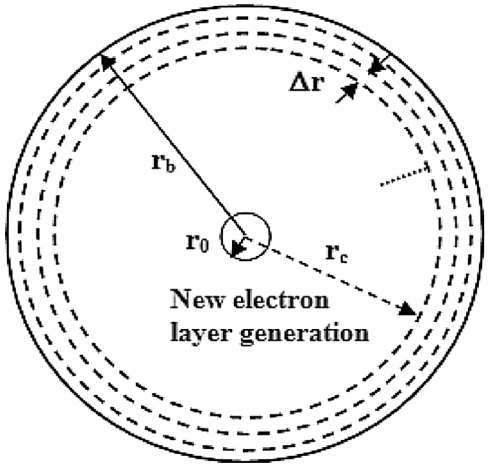

Fig. 1. Processes of corona discharge.

$$C = \frac{\Delta Q}{\Delta V} = C_{cor} + C_0 \tag{13}$$

3. Implementation in ATP-EMTP

In the Thevenin type component the corona capacitance is similar to a true non-linear component, with the same restrictions. The input to the model from the circuit is its Thevenin equivalent (resistance matrix and voltage vector) for the current time step. The Type-94 component is seen by EMTP as an electrical black box connected to the circuit, and it illustrates how to add new electrical components to ATP using external subroutines through the non-delayed interface between Models and ATP provided by the Type-94 nonlinear components. The dynamic corona model described in the previous section is implemented in a new model, developed using MODELS simulation language Type-94 within the ATP-EMTP package [28]. Fig. 2 depicts the interaction of a model with the rest of the simulated circuit when a Thevenin type-94 circuit component is utilized, and in which the previous equations describing the nonlinear corona are introduced. In the proposed model, the impulse overvoltage impinging on the line conductor is represented by an impulse voltage source of Heidler type to represent the case of lightning incidence, or a double-exponential type to represent the case of a switching operation, or a (1-cosine) damped oscillatory type to represent non-standard overvoltage. In this way, the proposed model is a useful contribution for the computation of travelling overvoltage surges on transmission lines in that it can be directly incorporated as a circuit component in transmission line networks considering the non-linear behavior of the corona effect at each time step of the overvoltage surge. In addition, the model considers non-standard and multiple impulse overvoltages, which have so far been given little attention in the published literature.

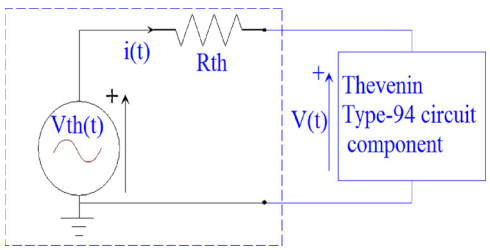

Fig. 2. Interface between a Thevenin type-94 circuit component of ATP-EMTP and the remaining of the simulated circuit.

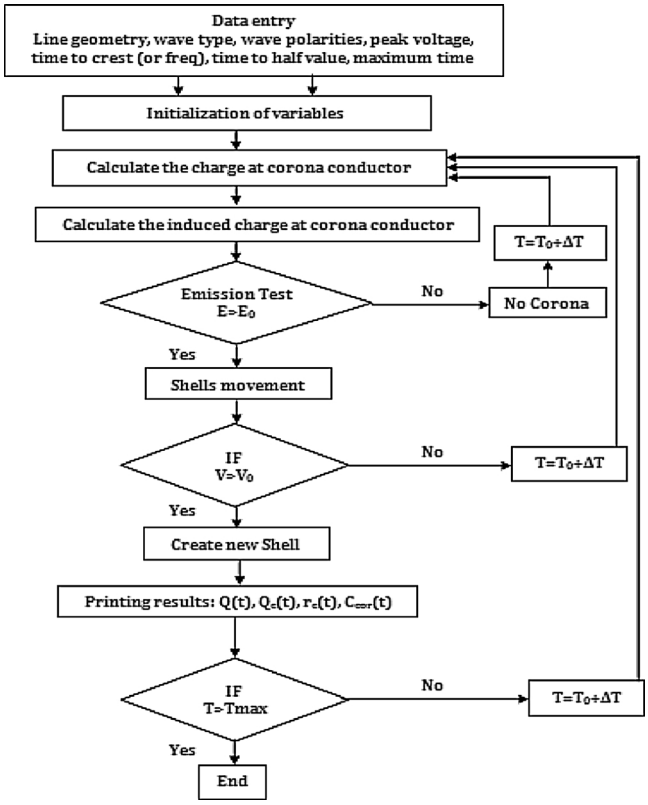

Fig. 3. Corona model calculation flow chart.

4. Simulation results

The computation procedure based on the model equations described in Section 3 and incorporated in the ATP/EMTP program is described in the flow chart shown in Fig. 3. The solution is obtained be simultaneously with the network by MODELS language using the numerical solution of trapezoidal rule of integration.

To validate the proposed model, the results are compared with published data using coaxial cylinder geometry where the inner conductor is subject to double exponential lightning impulses and unipolar oscillatory impulses. For this geometry, the charge–voltage curves are computed for different inner conductor radii and compared with those measured. The model is further applied to a conductor above-ground configuration for which the effect of conductor height on the computed charge–voltage curves is examined.

4.1. Q–V characteristics under impulse voltage

4.1.1. Coaxial conductor configuration

For the coaxial-conductor configuration, the inner and outer radii are 0.475 cm and 29.05 cm respectively. An impulse voltage of 250 kV peak and 2.5/60 μs is applied to enable direct comparison with the experiments reported in Ref. [14] for a positive polarity. Fig. 4 shows excellent agreement between the model results and the measured results. The corona inception voltage predicted by the model is V_0 = 121.11 kV, which compares with the measured value of V_0 = 119 kV. For $V \leq V_0$, the Q–V characteristic is linear with a constant slope representing the geometric capacitance. For $V > V_0$, the curve is non-linear with a variable slope representing the dynamic capacitance. The model can be extended for use with bundle-conductors. Fig. 5 shows the results of the charge–voltage curve computed for a two-conductor bundle having a conductor diameter of 12.5 mm and axial separation between bundles of 100 mm, in a coaxial configuration with 581 mm outer diameter. The applied voltage is a 300-kV, 120/

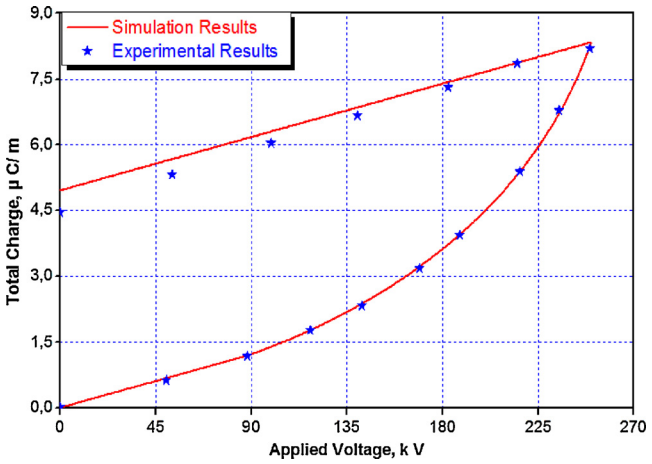

Fig. 4. Calculated and measured [14] Q–V curves for a single conductor in a coaxial geometry.

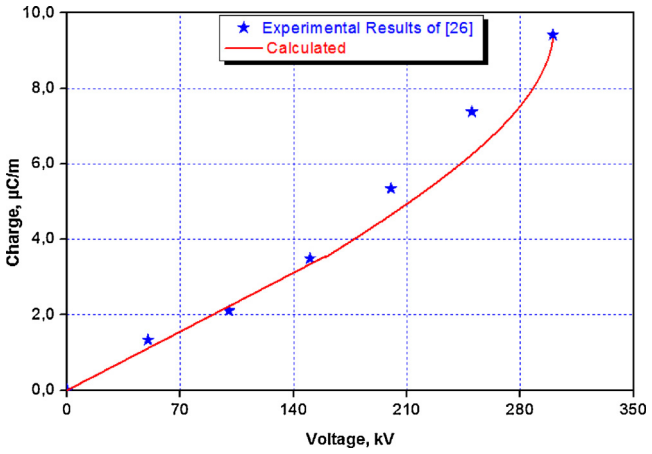

Fig. 5. Charge–voltage characteristic for a two-bundle conductor in a coaxial configuration.

2200 μs switching impulse voltage. As can be seen in the figure, there is a general agreement with the measurements reported in Ref. [26] using the same configuration. The inception voltage computed using the model is 159.5 kV, which is about 6% smaller than the measured voltage of 169 kV. The discrepancy between the model prediction and the measured curve may be because the inception voltage was computed based on Eq. (3) and the computed pre-corona field on the bundle conductor surface, which is applicable to single conductors. However, this can be considered acceptable since the inception field is essentially a function of the radius of curvature of the conductor in the bundle. Note also that the measurements reported in Ref. [26] are the averages of several voltage applications at a given voltage level, and hence are not a representative single charge–voltage relationship at that voltage level.

Fig. 6 shows the Q–V curves obtained with two single conductors of different diameters, namely 0.475 cm and 1.525 cm for the same applied voltage of 2.5/60 μs shape and 400 kV peak. As expected, the increase of conductor size results in a smaller corona charge being generated, and hence a smaller corona loss, which is due to the increase of corona inception voltage.

Comparison between model results and published experimental and theoretical data:

For the purpose of comparison with the experimental results reported in Ref. [29], a positive corona with the coaxial configuration with r_0 = 1.525 cm is used, and the results are shown in Table 1. As shown in the table, the model is in acceptable agreement with the

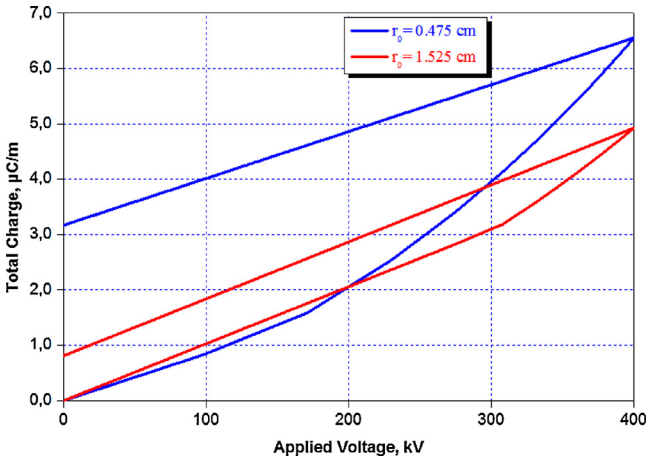

Fig. 6. Effect of conductor radius.

Table 1
Comparison of results with measurements and published data.

Impulse type	Applied voltage peak (kV)	Total apparent corona charge flow at impulse peak (μC/m)		
		Calculated (this model)	Measured [29]	Calculated [6]
−2.5/60 μs	290	3.12	3.6	3.5
	340	4.07	4.6	4.5
	390	5.20	6.6	5.3
	440	6.55	8	6.3
−260/2700 μs	290	3.11	3.4	3.6
	340	4.07	4.7	4.6
	390	5.21	5.7	5.4
	440	6.56	6.5	6.2

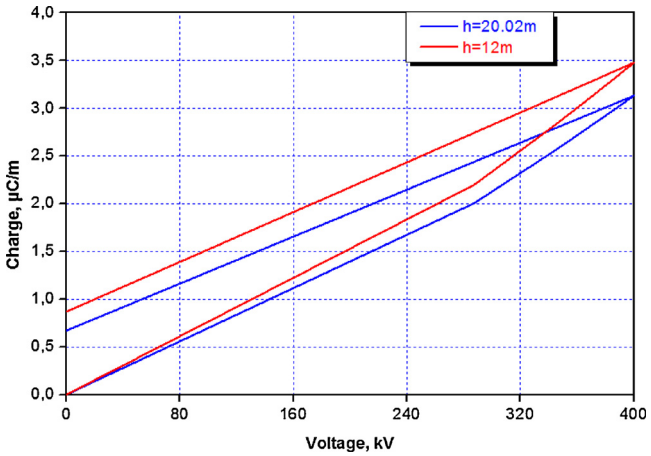

Fig. 7. Effect of conductor height.

experimental results. The values calculated from the model developed in Ref. [6] are also included for comparison.

4.1.2. Conductor above ground configuration

For the conductor-above-ground configuration, Fig. 7 illustrates the effect of conductor height on the Q–V curves, for a conductor radius of 0.475 cm at heights of 12 m and 20.02 m respectively, for an applied impulse voltage of 400 kV. The increase in conductor height causes a reduction of the capacitance to ground of the line, resulting in a reduction of the corona charge. An increase in the conductor height also causes a relatively small change in the corona onset voltage.

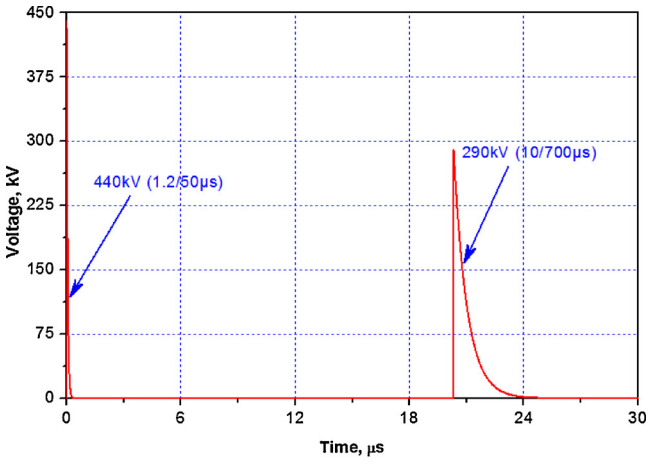

(a)

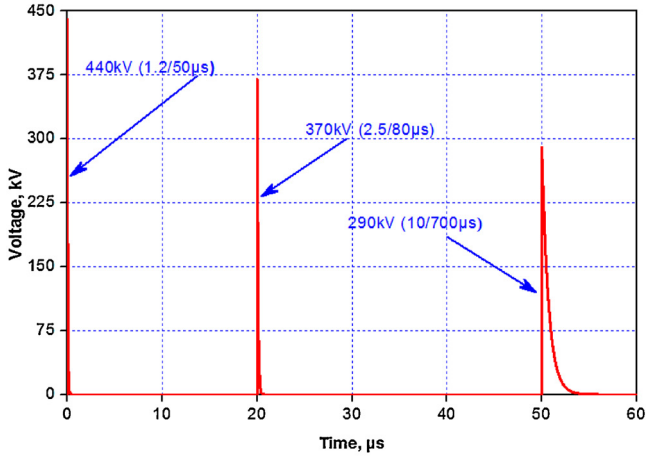

(b)

Fig. 8. Voltage and charge records with: (a) double exponential impulse, (b) voltage with three successive impulses.

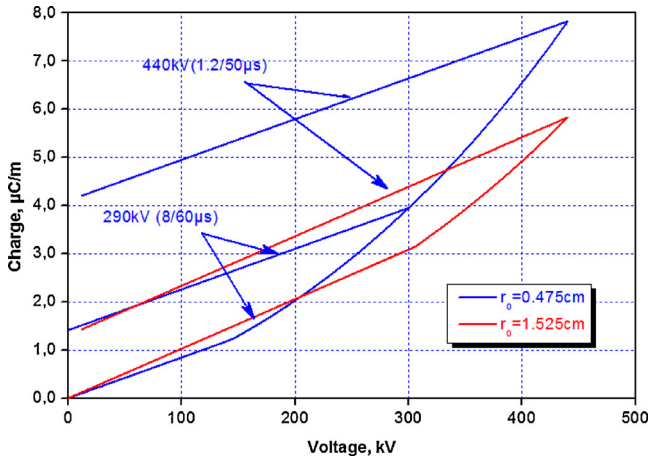

Fig. 9. Effect of conductor size on the corona charge.

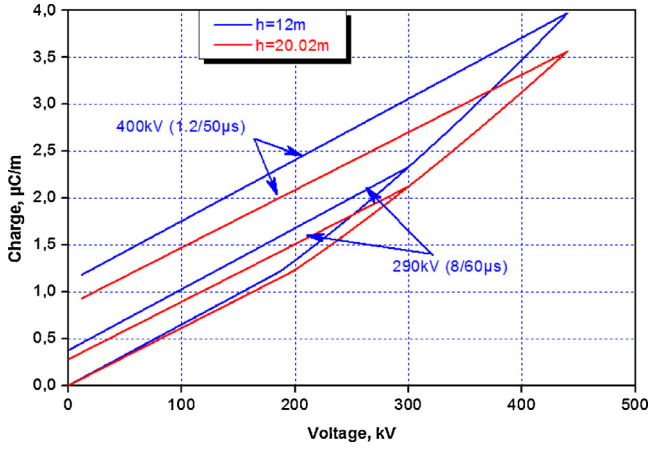

Fig. 10. Effect of conductor height on Q–V characterestics, conductor abobe ground configuration.

4.2. Application to the case of multiple impulse overvoltages

In practice, transmission lines can be affected by multiple lightning strikes. To simulate multiple lightning strikes occurring on the line, the conductor was energized with double exponential impulse voltage. The first impulse had a 1.2/50 μs waveshape and 440 kV magnitude and the second impulse had an 10/700 μs waveshape and 290 kV magnitude occurring at 20 ms after the first wave. These impulses are shown in Fig. 8(a) however in Fig. 8(b) shows the voltage with three successive impulses. A set of typical computed Q–V curves under double exponential impulses are shown in Figs. 9 and 10 for a coaxial configuration (inner radius: r_0 = 0.475 cm, and 1.525 cm and outer radius r_b = 29.05 cm) and conductor above-ground configuration (h = 12 and 20.02 m) respectively.

In Fig. 9, the charge–voltage curve for the double-stroke lightning impulse shows that for the intense first stroke, corona appears and the charge reaches the maximal value of 7.8 μC around the conductor of 0.475 cm radius, but reaches only 3.8 μC for the second stroke. For the larger conductor of 1.525-cm radius, the maximum charge is 5.8 μC following the first stroke and 2.8 μC following the second stroke. For this conductor, corona does not occur during the second stroke.

For the case of the conductor above the ground configuration, Fig. 10 shows that corona takes place during both the first and the second stroke, and the generated charge is lower the higher the conductor. This is significant for unshielded transmission lines where corona attenuation may not be sufficient to reduce the lightning overvoltage to safe levels. In such cases, the use of lightning line arresters may be required. For distribution lines with lower conductor heights, corona attenuation should be relatively more important, and hence line arresters are only required at the transformer terminals.

4.3. Q–V characteristics under oscillatory impulse

To analyze the behavior of corona discharge under complex non-standard impulse overvoltage, a damped oscillatory impulse voltage is considered. This voltage is computed in MODELS interface, and is described by the following equation.

$$V = K.\ V_{\max}\left(1 - e^{-\alpha(t-t_0)}\cos(2\pi f\,(t - t_0))\right) \tag{14}$$

where:

K: Correction coefficient

V_{max}: Peak voltage value, in [kV]

t_0: The initial instant of application of the overvoltage in [μs]

t: Is the surge wavelength, in [μs].

An example of the voltage waveform is shown in Fig. 11 with a peak value of 400 kV.

The dynamic charge–voltage curve for an oscillatory impulse of 400 kV applied to the coaxial geometry of r_0 = 0.475 cm, r_b = 29,05 cm, is shown in Fig. 12. For the ascending part of the curve (portion OAB), the total charge varies in a manner similar to that observed under double exponential impulses. Following corona extinction, this occurs when the voltage falls below inception value in the first oscillation, the portion (BC) of the curve falls with a slope

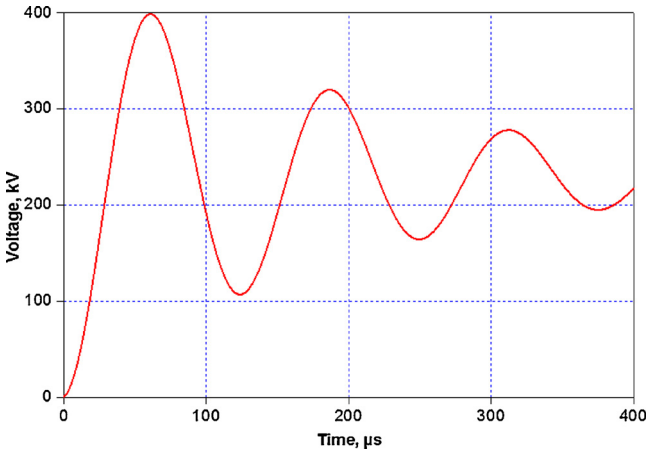

Fig. 11. Damped oscillatory impulse voltage.

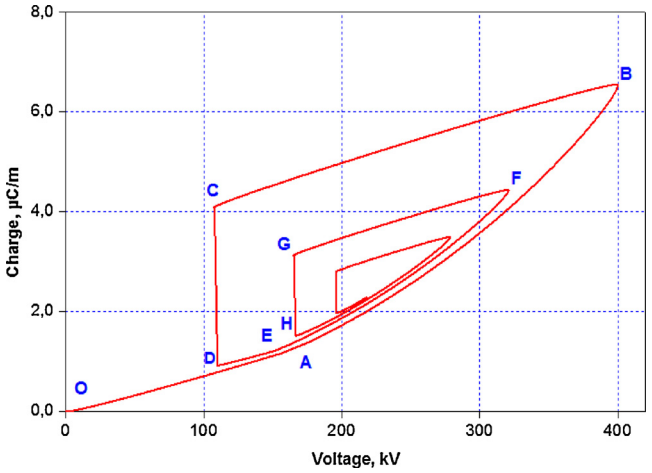

Fig. 12. Charge–voltage curve for an oscillatory impulse voltage.

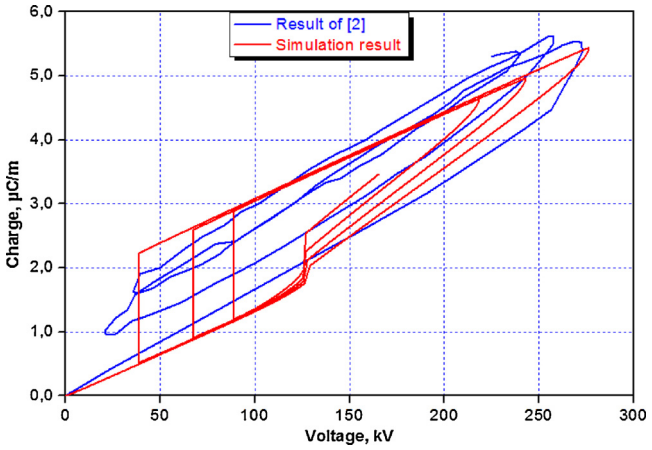

Fig. 13. Dynamic charge–voltage curves, 33 kHz impulse, 270 kV.

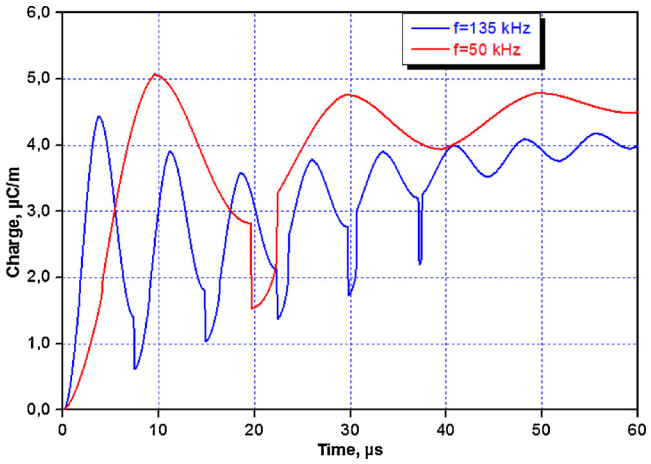

Fig. 14. Charge variation under frequency of 50 kHz and 135 kHz.

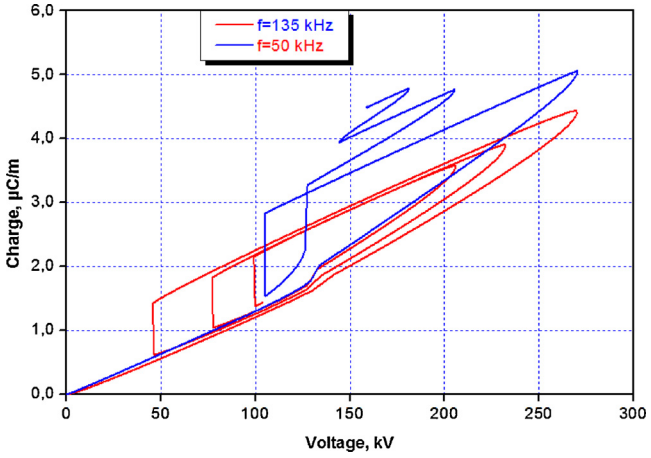

Fig. 15. Effect of frequency on the Q–V characteristics.

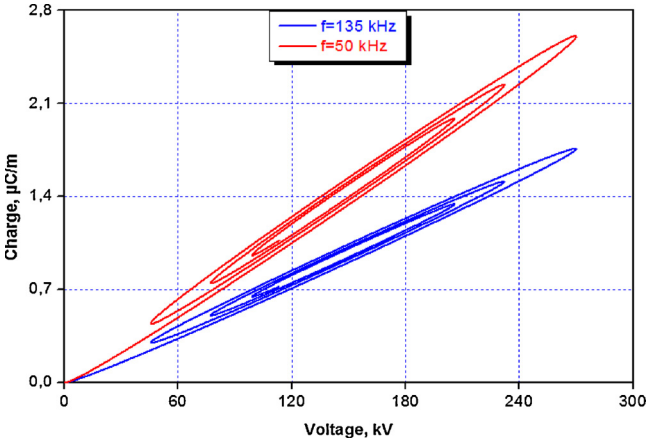

Fig. 16. Effect of frequency on Q–V curves for conductor above the ground configuration.

approximately equal to that of portion OA, i.e. the geometrical capacitance.

The large reduction in charge observed (portion CD) is due to the occurrence of reverse corona generating a charge of opposite polarity drifting towards the conductor. These reverse coronas occur near or at voltage minima. The corona activity during the subsequent voltage cycles consists of a process where bipolar coronas take place, with the negative coronas occurring at the voltage maxima and the reverse (positive) coronas taking place at the voltage minima. This gives the Q–V curve a distinct feature showing large loops with a continuous increase in corona charge after successive voltage peaks due to space charge drift away from the electrode. The reduction in charge due to reverse corona is dependent on the mobility of the space charge towards the conductor.

4.3.1. Comparison with experimental results

The model is tested by comparing the results to experimental results

described in Ref. [2] for a coaxial-conductor configuration. As shown in Fig. 13 for oscillatory voltage of 270 kV and 33 kHz oscillatory impulse, the model is able to reproduce the corona charge behavior over the first few cycles, and the corona charge peak on the first cycle. However, some differences exist on the rising parts and falling parts of the curve, presumably due to the approximations made in the model. Also, since the model does not take into account the charge drift following corona extinction, it is not showing an increase in charge on the rising part of subsequent cycles. More detailed modelling is required to replicate this behavior.

4.3.2. *Effect of oscillatory impulse frequency*

The effect of frequency on the time variations of the corona charge was considered for a coaxial conductor configuration with 0.475 cm inner conductor radius, and outer cylinder radius of 29.05 cm. The curves shown in Fig. 14 illustrates the variation of charge at the inner conductor for two oscillatory impulse voltages having the same amplitude of 270 kV, and different frequencies 50 kHz and 135 kHz. The reverse corona seems to occur more with the 135 kHz oscillatory impulse than the 50 kHz impulse. This can be explained by the higher voltage gradients developing during the falling part of each cycle, creating an opposite-polarity space charge field. This field acts against charge growth causing a sudden decrease in charge as observed in the figure. This reverse corona occurs only in the falling part of the first cycle for slower oscillatory impulse of 50 kHz. The forward corona in the subsequent cycles behaves in a similar manner, creating an increase in charge according to the constraints set in the model. In reality, as was observed with the experimental results shown in Fig. 14, the reduction in charge near the voltage minima does not occur abruptly, and a refinement of the model is needed to account for this change. The charge–voltage curves associated with these two impulses are shown in Fig. 15.

The charge–voltage corona curves for the conductor of 0.475 cm radius above ground at h = 12m, for frequencies of 50 kHz and 135 kHz and peak value of 270 kV, are shown in Fig. 16. In this case also, the charge for the higher-frequency oscillatory impulse is higher than that with lower-frequency impulse.

5. Conclusions

A dynamic corona model for the simulation of the non-linear characteristics of impulse corona discharge has been developed. The model is used for computation of surge propagation on transmission lines that occur under standard and non-standard lightning impulses by implementation in ATP-EMTP software using MODELS simulation language. With the aid of a type-94 circuit component, the new model is solved simultaneously with the rest of system interacting with it as a circuit element. The model is able to compute the charge–voltage characteristics and space charge due to corona phenomenon. This has been adopted because complex networks and control systems can be simulated in EMTP, which is a suitable tool for lightning overvoltage analysis.

It provides a means for an accurate estimation of corona characteristics with the proposed model for a coaxial-conductor configuration and a conductor above ground configuration under multiple and non-standard impulses.

The model is validated by comparing its results with the experimental results available in the literature. To make certain the validity of the proposed model, it is intended, as a future work, to introduce the present model as an additional capacitance in a transmission line distributed-parameter model and analyse the propagation of traveling waves due to lightning impulse, with changing pressure and humidity and compare with the related measured data.

References

[1] X. Bian, D. Yu, X. Meng, M. MacAlpine, L. Wang, Z. Guan, W. Yao, S. Zhao, Corona-generated space charge effects on electric field distribution for an indoor corona cage and a monopolar test line, IEEE Trans. Dielectr. Electr. Insul. 18 (5) (2011).

[2] N. Harid, Impulse Voltage Testing of Phase Conductor Models, Cardiff University, 1990.

[3] X.-R. Li, O.P. Malik, Z.-D. Zhao, Computation of transmission line transients including corona effects, IEEE Trans. Power Deliv. 4 (3) (1989) 1816–1822.

[4] C. Gary, A. Timotin, D. Cristescu, Prediction of surge propagation influenced by corona and skin effect, IEE Proc. A - Phys. Sci. Meas. Instrum. Manag. Educ. Rev. 130 (5) (1983) 264–272.

[5] T.J. Gallagher, I.M. Dudurych, Model of corona for an EMTP study of surge propagation along HV transmission lines, IEE Proc. Gener. Transm. Distrib. 151 (1) (2004) 61–66.

[6] D.A. Rickard, N. Harid, R.T. Waters, Modelling of corona at a high-voltage conductor under double exponential and oscillatory impulses, IEE Proc. Sci. Meas. Technol. 143 (5) (1996) 277–284.

[7] M. Abdel-salam, E.K. Stanek, Mathematical-physical model of corona from surges on high-voltage lines, IEEE Trans. Ind. Appl. IA-23 (3) (1987) 481–489.

[8] J. He, P. Yang, S. Chen, R. Zeng, Lightning impulse corona characteristic of 1000 kv UHV transmission lines, 2013 Int. Symp. Light. Prot. SIPDA 2013, no. 2009 (2013) 108–112.

[9] T.H. Thang, Y. Baba, N. Nagaoka, A. Ametani, N. Itamoto, V.A. Rakov, FDTD simulation of direct lightning strike to a phase conductor: influence of corona on transient voltages at the tower, Electr. Power Syst. Res. 123 (2015) 128–136.

[10] J. He, X. Zhang, P. Yang, S. Chen, R. Zeng, Attenuation and deformation characteristics of lightning impulse corona traveling along bundled transmission lines, Electr. Power Syst. Res. 118 (2015) 29–36.

[11] N. Harid, D.M. German, R.T. Waters, Characteristics of corona discharge under oscillatory impulse voltages', Proc. 25th Universities Power Engineering Conference (UPEC) (1990).

[12] H. Wei-Gang, W. Xiao-Ping, Corona QV characteristics under unipolar-damped oscillating impulses [substations], IEEE Trans. Dielectr. Electr. Insul. 4 (6) (1997) 758–762.

[13] X.Q. Zhang, Study on corona characteristics under nonstandard lightning impulses, Electr. Eng. 89 (7) (2007) 519–524.

[14] M.A. Al-Tai, H.S.B. Elayyan, D.M. German, A. Haddad, N. Harid, R.T. Waters, The simulation of surge corona on transmission lines, IEEE Trans. Power Deliv. 4 (2) (1989) 1360–1368.

[15] K. Huang, X. Zhang, An experimental study on corona q–u curves under non-standard lightning impulses, J. Electrostat. 81 (2016) 37–41.

[16] P. Yang, S. Chen, J. He, Lightning impulse corona characteristic of 1000-kV UHV transmission lines and its influences on lightning overvoltage analysis results, IEEE Trans. Power Deliv. 28 (4) (2013) 2518–2525.

[17] J. Wang, X. Wang, Lightning transient simulation of transmission lines considering the effects of frequency dependent and impulse corona, 2011 International Conference on Electrical and Control Engineering (ICECE) (2011) 696–699.

[18] A. Zangeneh, A. Gholami, V. Zamani, A new method for calculation of corona inception voltage in stranded conductors of overhead transmission lines, Power and Energy Conference, 2006. PECon'06. IEEE International (2006) 571–575.

[19] N. Harid, R.T. Waters, Statistical study of impulse corona inception parameters on line conductors, IEE Proc. A - Sci. Meas. Technol. 138 (3) (1991) 161–168.

[20] K. Huang, X. Zhang, An experimental study on corona qu curves under non-standard lightning impulses, J. Electrostat. 81 (2016) 37–41.

[21] E.I. Bousiou, P.N. Mikropoulos, V.N. Zagkanas, Application of the critical volume theory to estimating impulse corona characteristics in the coaxial cylindrical electrode arrangement, Universities Power Engineering Conference (UPEC), 2017 52nd International (2017) 1–5.

[22] P.N. Mikropoulos, V.N. Zagkanas, Impulse corona inception in the coaxial cylindrical electrode arrangement in air: effects of the steepness of the applied voltage, Proc. 18th International Symposium on High Voltage Engineering, Seoul, South Korea, paper No. PE-50, 2013.

[23] P.N. Mikropoulos, V.N. Zagkanas, Threshold inception conditions for positive DC corona in the coaxial cylindrical electrode arrangement under variable atmospheric conditions, IEEE Trans. Dielectr. Electr. Insul. 22 (1) (2015) 278–286.

[24] P.N. Mikropoulos, V.N. Zagkanas, Negative DC corona inception in coaxial cylinders under variable atmospheric conditions: a comparison with positive corona, IEEE Trans. Dielectr. Electr. Insul. 23 (3) (2016) 1322–1330.

[25] G.J. Reid, H.J. Vermeulen, Effects of conductor temperature on corona inception, 2014 49th International Universities Power Engineering Conference (UPEC), Cluj-Napoca, 2014, pp. 1–5, , http://dx.doi.org/10.1109/UPEC.2014.6934700.

[26] D.M. German, R.T. Waters, N. Harid, M.A. Altai, Impulse corona tests on single and bundle conductors, Sixth International Symposium on High Voltage Engineering, New Orleans, USA, 1989, pp. 1–4.

[27] P.S. Maruvada, R.J. Bacha, A.C. Backer, W.E. Blair, M.E. Bulawka, V.I. Chartier, R. Cortins, L.S. Craine, G.R. Elder, C. Gary, A survey of methods for calculating transmission line conductor surface voltage gradients, IEEE Corona F. Eff. Subcomm. Rep. Radio Noise Work. Gr. Power Appar. Syst. v. PAS 93 (1979) 1660–1668.

[28] H.W. Dommel, Electromagnetic Transients Program: Reference Manual: (EMTP Theory Book), Bonneville Power Administration, 1986.

[29] P.S. Maruvada, H. Menemenlis, R. Malewski, Corona characteristics of conductor bundles under impulse voltages, IEEE Trans. Power Appar. Syst. 96 (1) (1977) 102–115.